error), 0.07 (off-resonant excitations), 0.04 (laser frequency noise (200 Hz r.m.s.)). Another possible error source is imperfect ground state cooling. Intensity noise of the 729-nm laser ($\Delta I_{max}/I = 0.03$) does not contribute significantly. Finally, we experimentally observed non-ideal optical pumping, which can result in a reduction of 0.02 of the fidelity per ion. In principle, this imperfection can be eliminated by single ion detection and subsequent π pulses on the carrier transition. Currently, for $N \geq 6$, we reduce the errors due to optical pumping and a part of the addressing errors by checking the initialization procedure with a detection sequence (see Table 1).

1. Schrödinger, E. Die gegenwärtige Situation in der Quantenmechanik. *Naturwissenschaften* 23, 807–812 (1935).
2. Schrödinger, E. Die gegenwärtige Situation in der Quantenmechanik. *Naturwissenschaften* 23, 823–828 (1935).
3. Schrödinger, E. Die gegenwärtige Situation in der Quantenmechanik. *Naturwissenschaften* 23, 844–849 (1935).
4. Sackett, C. A. *et al.* Experimental entanglement of four particles. *Nature* 404, 256–259 (2000).
5. Zhao, Z. *et al.* Experimental demonstration of five-photon entanglement and open-destination teleportation. *Nature* 430, 54–58 (2004).
6. Dür, W., Vidal, G. & Cirac, J. I. Three qubits can be entangled in two inequivalent ways. *Phys. Rev. A* 62, 062314 (2000).
7. Zeilinger, A., Horne, M. A. & Greenberger, D. M. Higher-order quantum entanglement. *NASA Conf. Publ.* 3135, 73–81 (1992).
8. Roos, C. F. *et al.* Control and measurement of three-qubit entangled states. *Science* 304, 1478–1480 (2004).
9. Bennett, C. H. & DiVincenzo, D. P. Quantum information and computation. *Nature* 404, 247–255 (2000).
10. Roos, C. F. *et al.* Bell states of atoms with ultralong lifetimes and their tomographic state analysis. *Phys. Rev. Lett.* 92, 220402 (2004).
11. Greenberger, D. M., Horne, M. A. & Zeilinger, A. in *Bell's Theorem, Quantum Theory, and Conceptions of the Universe* (ed. Kafatos, M.) 69–72 (Kluwer Academic, Dordrecht, 1989).
12. Leibfried, D. *et al.* Creation of a six-atom 'Schrödinger cat' state. *Nature* doi:10.1038/nature04251 (this issue).
13. Briegel, H. J. & Raussendorf, R. Persistent entanglement in arrays of interacting particles. *Phys. Rev. Lett.* 86, 000910 (2001).
14. Sen(De), A. *et al.* Multiqubit W states lead to stronger nonclassicality than Greenberger–Horne–Zeilinger states. *Phys. Rev. A* 68, 062306 (2003).
15. Joo, J., Park, Y.-J., Lee, J., Jang, J. & Kim, I. Quantum secure communication via a W state. *J. Korean Phys. Soc.* 46, 763–768 (2005).
16. Joo, J., Lee, J., Jang, J. & Park, Y.-J. Quantum secure communication with
W States. Preprint at ⟨http://arxiv.org/quant-ph/0204003⟩ (2002).
17. Buhrman, H., van Dam, W., Heyer, P. & Tapp, A. Multiparty quantum communication complexity. *Phys. Rev. A* 60, 2737–2741 (1999).
18. Schmidt-Kaler, F. *et al.* How to realize a universal quantum gate with trapped ions. *Appl. Phys.* B77, 789–796 (2003).
19. Fano, U. Description of states in quantum mechanics by density matrix and operator techniques. *Rev. Mod. Phys.* 29, 74–93 (1957).
20. Hradil, Z., Řeháček, J., Fiurášek, J. & Ježek, M. Maximum-likelihood methods in quantum mechanics. *Lect. Notes Phys.* 649, 59–112 (2004).
21. Horodecki, M., Horodecki, P. & Horodecki, R. Separability of mixed states: Necessary and sufficient conditions. *Phys. Lett. A* 223, 1–8 (1996).
22. Terhal, B. M. Bell inequalities and the separability criterion. *Phys. Lett. A* 271, 319–326 (2000).
23. Bourennane, M. *et al.* Experimental detection of multiparticle entanglement using witness operators. *Phys. Rev. Lett.* 92, 087902 (2004).
24. Dür, W. & Cirac, J. I. Classification of multiqubit mixed states: Separability and distillability properties. *Phys. Rev. A* 61, 042314 (2000).
25. Wootters, W. K. Entanglement of formation of an arbitrary state of two qubits. *Phys. Rev. Lett.* 80, 2245–2248 (1998).
26. Miyake, A. & Briegel, H.-J. Distillation of multipartite entanglement by complementary stabilizer measurements. Preprint at ⟨http://arxiv.org/quant-ph/0506092⟩ (2005).
27. Dür, W. & Cirac, J. I. Multipartite entanglement and its experimental detection. *J. Phys. A* 34, 6837–6850 (2001).
28. Koashi, M., Bužek, V. & Imoto, N. Entangled webs: Tight bound for symmetric sharing of entanglement. *Phys. Rev. A* 62, 050302 (2000).
29. Gulde, S. *et al.* Implementing the Deutsch–Jozsa algorithm on an ion-trap quantum computer. *Nature* 421, 48–50 (2003).

Origin of the metallic properties of heavily boron-doped superconducting diamond

T. Yokoya[1,2], T. Nakamura[1], T. Matsushita[1], T. Muro[1], Y. Takano[3], M. Nagao[3], T. Takenouchi[4], H. Kawarada[4] & T. Oguchi[5]

The physical properties of lightly doped semiconductors are well described by electronic band-structure calculations and impurity energy levels[1]. Such properties form the basis of present-day semiconductor technology. If the doping concentration n exceeds a critical value n_c, the system passes through an insulator-to-metal transition and exhibits metallic behaviour; this is widely accepted to occur as a consequence of the impurity levels merging to form energy bands[2]. However, the electronic structure of semiconductors doped beyond n_c have not been explored in detail. Therefore, the recent observation of superconductivity emerging near the insulator-to-metal transition[3] in heavily boron-doped diamond[4,5] has stimulated a discussion on the fundamental origin of the metallic states responsible for the superconductivity. Two approaches have been adopted for describing this metallic state: the introduction of charge carriers into either the impurity bands[6] or the intrinsic diamond bands[7–9]. Here we show experimentally that the doping-dependent occupied electronic structures are consistent with the diamond bands, indicating that holes in the diamond bands play an essential part in determining the metallic nature of the heavily boron-doped diamond superconductor. This supports the diamond band approach and related predictions, including the possibility of achieving dopant-induced superconductivity in silicon and germanium[7]. It should also provide a foundation for the possible development of diamond-based devices[10].

An accurate description of the overall electronic structure is extremely important for understanding the mechanism of the superconductivity. We can approach this in two ways. First, we consider a localized picture that evolves into a metallic state in the vicinity of the insulator-to-metal transition. In diamond, carbon atoms are crystallized into a $2s2p^3$ three-dimensional network with covalent bonding. The resulting band structure[11] has a large valence bandwidth (22 eV); its top is located at the Γ point in the Brillouin zone (BZ) and is separated from the bottom of the conduction band with a 5.5-eV bandgap. For low carrier concentration, boron atoms probably replace the carbon sites by substitution and form an impurity level with an activation energy of 0.37 eV (ref. 12). As the boron concentration is increased, the wavefunctions of holes bound to an impurity site can overlap and the impurity level evolves into an impurity 'band'. The holes in a nearly localized 'band' are strongly affected by Coulomb forces, owing to small screening effects, and so electron–electron correlation is important. Both this and an extended s-wave superconductivity due to electron correlation were predicted in ref. 6. For the second approach, we consider the extended picture for the metallic states, starting from the diamond band structure. The doped holes lead to depopulation of the bands

with a dominant diamond character hybridized with boron states. Recent theoretical studies based on band structure calculations predicted that the superconductivity is driven by phonons strongly coupled to holes at the Γ point[7–9].

To distinguish the two scenarios we need to experimentally determine the band dispersion near the Fermi level E_F. To do this, we performed angle-resolved photoemission spectroscopy (ARPES) with the ability to measure band dispersions of crystalline solids. The intensity at E_F of normal-incidence ARPES spectra from a single-crystal diamond (111) film (BDD1) using photon energies from 770 to 870 eV were mapped with blue colour in Fig. 1a, which is a cross-section of the BZ for the diamond structure (Fig. 1b), including the ΓKLUX plane. The intensity distribution exhibits a maximum around the Γ point, consistent with the fact that diamond has a valence band maximum at the Γ point. Figure 1c shows an ARPES intensity map of BDD1 along the red curve in the ΓKLUX plane of the BZ (Fig. 1a) using a photon energy of 825 eV. ARPES using a soft X-ray (SXARPES) provides bulk sensitive band structures compared with vacuum ultraviolet ARPES[13], but may have a larger window of momentum k parallel to the surface normal k_n, owing to larger available final states[14].

In Fig. 1c, several dispersive features corresponding to experimentally obtained bands can be seen (denoted A–G). For the region of lower binding energy, we observe three dispersive features (A, B and C), all of which disperse towards E_F and appear to locate very close to E_F at Γ (we will discuss the band dispersion near E_F later in detail). Band C seems to disperse up to a binding energy of 14 eV and has an energy minimum at around 1.5 Å^{-1}. At regions of higher binding energy, we observe higher-intensity features on both sides of Γ (D and E), suggesting a parabolic dispersion with a minimum at Γ. Band D seems to have a dispersion peak at around 1.5 Å^{-1}, forming a bandgap with band C at a zone boundary. We also see an intensive feature (F) with nearly straight dispersion and a non-dispersive feature (F) at 13 eV (G).

To compare the experimental bands with calculations, in Fig. 1d we show the same ARPES intensity map as in Fig. 1c superimposed with calculated band dispersions (solid white lines) along the red curve shown in Fig. 1a. The broken white lines are those calculated along the green line in Fig. 1a, shifted by the surface reciprocal lattice vector G. The calculated dispersions are energy-expanded by 10% and tentatively aligned so that the top of the valence band is located at 0.40 eV above E_F. We found that the experimental band dispersions (A, B, C, D and E) are very similar to the calculated band dispersions, including the bandgap at the zone boundary. Band F looks similar to the some of the broken lines and may thus be attributed to the surface umklapp band. The non-dispersive band G is not described with the

[1]Japan Synchrotron Radiation Research Institute (JASRI/SPring-8, 1-1-1 Kouto, Sayo, Hyogo 679-5198, Japan. [2]The Graduate School of Natural Science and Technology, Okayama University, 3-1-1 Tsushima-naka, Okayama 700-8530, Japan. [3]National Institute for Materials Science, 1-2-1 Sengen, Tsukuba, Ibaraki 305-0047, Japan. [4]School of Science and Engineering, Waseda University, 3-4-1 Okubo, Shinjuku, Tokyo 169-8555, Japan. [5]Department of Quantum Matter, Graduate School of Advanced Sciences of Matter (ADSM), Hiroshima University, 1-3-1 Kagamiyama, Higashi-Hiroshima 739-8530 Japan.
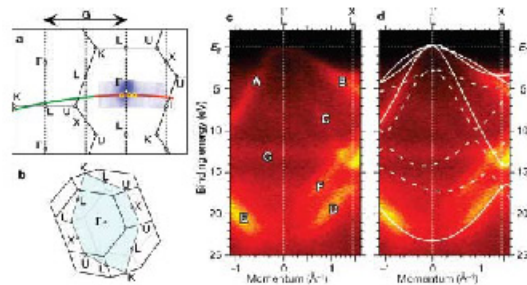
Figure 1 | Experimentally determined valence-band dispersions and the BZ of diamond. a, Two-dimensional BZ showing estimated measured k positions for the states near E_F (a red curve). The intensities near E_F from photon energy (770–870 eV) dependent SXARPES spectra from a single-crystal diamond (111) film are mapped with blue colour (higher spectral intensity corresponds to dense colour). The measured k positions are determined with a free-electron final-state model using:

$$\langle h/2\pi\rangle k_\perp = [2m(E\cos^2\theta + V_0)]^{1/2} - k_{\perp photon}.$$

where h is Planck's constant, m is the electron mass, E and θ are the kinetic energy and the polar angle of an emitted photoelectron, and $k_{\perp photon}$ is the surface normal momentum component of the photon. G is the surface reciprocal lattice vector. The yellow circles are k_F values determined from the MDC analysis. **b,** Three-dimensional BZ for the f.c.c. diamond crystal. The pale-blue plane includes the measured k positions shown in **a**. **c,** A valence-band SXARPES intensity map from a single-crystal diamond (111) film using a photon energy of 825 eV. **d,** Comparison of the same SXARPES intensity map with calculated band dispersions of diamond (white full and broken lines) along the red and green curves in **a**.

calculated dispersions, but may be related to the sharp s–p-band-derived density of states (DOS) observed from previous X-ray photoemission spectroscopy[15], such as for the SXARPES of graphite[16]. These indicate that the gross electronic structure of diamond is retained with heavy boron doping.

As mentioned above, we find that the highly dispersive bands approach very close to E_F in Fig. 1c. To look more carefully at the states near E_F we performed another SXARPES measurement for BDD1 with a smaller step size and with a higher signal-to-noise ratio, as shown in Fig. 2a. We now see the three bands near E_F more clearly and find that they disperse across E_F, as is evident from a reduction of intensity along $k = 0$ near E_F. The band crossing can further be confirmed from the momentum distribution curve (MDC) at E_F, and at binding energies of 0.3, 0.6 and 0.9 eV with an energy window of ± 0.15 eV. These MDCs have a multiple-peak structure that can be well reproduced with three lorentzian functions, as shown in Fig. 2b. The k positions of the centres of the lorentzian functions for MDC at E_F correspond to the Fermi momenta ($k_F^A = -0.15 \pm 0.04$ Å^{-1}, $k_F^C = 0.11 \pm 0.02$ Å^{-1} and $k_F^B = 0.27 \pm 0.02$ Å^{-1}). These SXARPES results indicate that the observed diamond bands cross E_F, forming hole pockets at the Γ point. The observation that the experimentally obtained band dispersions are similar to those calculated motivates us to determine the position of E_F with respect to the top of the valence band of the diamond band. We found that a location of E_F at 0.40 ± 0.2 eV below the top of the valence band, as shown in Fig. 2c, was necessary to relate k_F^A, k_F^B and k_F^C to our band structure calculations (white lines). This corresponds to the region of the carrier concentration: 6.6×10^{20} cm$^{-3} < n = 1.9 \times 10^{21}$ cm$^{-3} < 4.4 \times 10^{21}$ cm^{-3}. These values are found to have a slightly lower value compared to the boron concentration from secondary ion mass spectroscopy (SIMS) measurements ($n_{B,SIMS} = 8.37 \times 10^{21}$ cm^{-3}).

To study the evolution of the states near E_F we performed additional near-E_F SXARPES for BDD2 and BDD3 with lower boron concentrations, as shown in Fig. 2d and e. In Fig. 2d, we observe clearer dispersions in BDD2 than in BDD1, indicative of a sharpening of electronic structures in BDD2. But the band dispersions are similar to each other overall. From the MDC analysis for BDD2 (Fig. 2f), we obtained values for the Fermi

momenta ($k_F^A = -0.09 \pm 0.01$ Å^{-1}, $k_F^C = 0.06 \pm 0.008$ Å^{-1} and $k_F^B = 0.19 \pm 0.007$ Å^{-1}). The smaller k_F values of BDD2 compared to those of BDD1 indicate that the number of carriers decreases with lowered boron concentration. We also found that a shift of 0.2 ± 0.1 eV is needed to match the band calculations to experimental k_F values, as shown in Fig. 2h. In Fig. 2e, the band dispersions of BDD3, which has a much lower boron concentration, are similar to those of BDD1 and BDD2 except near E_F. The results show a qualitative difference at the top of the band dispersion, where the plot for BDD3 has a local maximum at the Γ-point, while the plots for BDD1 and BDD2 show local minima at the Γ-point. This is consistent with the band structure calculation for E_F positioned just at the valence band maximum, as shown in Fig. 2i. This indicates that the bands of BDD3 do not cross E_F. We could not measure the band dispersion of pure diamond because of charging-up effects. However, the bandwidths estimated as a function of doping are 23.5 eV ± 0.5 eV for both BDD1 and BDD3, indicating that a bandwidth change cannot be discerned, which is in agreement with the experimental bandwidth of undoped diamond (23.0 $\pm$ 0.2 eV) (ref. 17).

It may be interesting to estimate fundamental physical parameters from the MDC analysis and compare those values from samples with different boron concentrations. For band A of BDD1 and BDD2, the mean free path values λ, estimated from the half-width at half-maximum of the lorentzian for MDC at E_F, are 5.3 and 8.6 Å. From fits to the peak positions for the four binding energies (0.0 (=E_F), 0.3, 0.6 and 0.9 eV), we obtain Fermi velocities $|v_F|$ of 7.9 and 7.0 eVÅ, which correspond to values for the lifetime of the carrier τ (=λ/v_F) of 2.8 and 5.1 fs for BDD1 and BDD2. We note that because diamond is a three-dimensional material, contributions from the final-state electron lifetime cannot be neglected. Therefore the obtained λ and τ values give its lowest limit. Nonetheless, this simple analysis indicates a shorter lifetime of carriers in BDD1 than in BDD2.

These results indicate that the doped holes in this hole-concentration region enter into the top of the diamond valence band, accompanied by a shift of E_F. This justifies the band approach to the metallic states of heavily boron-doped diamond. This is
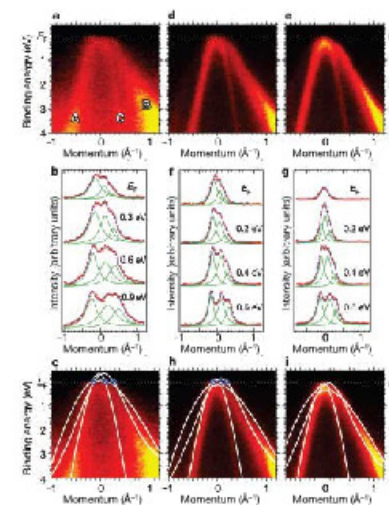

Figure 2 | Experimental band dispersions near E_F as a function of boron concentration and the results of MDC analysis. a, A near-E_F SXARPES intensity map from a single-crystal diamond (111) film (BDD1) using a photon energy of 825 eV along the red curve in Fig. 1a. **b,** MDCs at binding energies of 0.0 (= E_F), 0.3, 0.6 and 0.9 eV with an energy window of ± 0.15 eV (red dots) for BDD1. The blue line for each MDC is the sum of three lorentzians (green lines) corresponding to the three bands (A, B and C). **c,** A comparison of the experimental data with band structure calculations (white curves). k_F values determined from the MDC analysis are shown as blue circles. The white curves are the calculated band dispersion energies expanded 10% and shifted by 0.4 eV. That the calculated band dispersion splits at the top of the valence band corresponds to the measured k position, which is slightly away from the Γ point, as shown in Fig. 1a. The bands are indeed degenerate with the same valence-band maximum at the Γ point as for the calculated results of the Γ point. **d, e,** As for **a** but for BDD2 and BDD3, respectively. **f, g,** MDCs at binding energies of 0.0 (= E_F), 0.2, 0.4 and 0.6 eV with an energy window of ± 0.10 eV for BDD2 and BDD3, respectively, which emphasize the difference in MDC lineshapes in the near-E_F region. Descriptions for lines and symbols are the same as in **b**. Please note the very small intensity at E_F for BDD3 compared with the intensity at 0.2 eV for BDD3 as well as the intensity at E_F for BDD1 and BDD2, suggesting a qualitative difference in the E_F position. **h, i,** As for **c** but for BDD2 and BDD3, respectively. The energy-expanded calculated band dispersions are shifted by 0.2 eV for BDD2, but they are not shifted for BDD3.

different from the impurity band model[6] and recent X-ray absorption spectroscopy (XAS) studies interpreting holes in the valence band located at about 1.3 eV below the valence band maximum, regardless of the doping level[18]. However, XAS measures site-projected, angular-momentum-projected unoccupied DOS in the presence of an attractive core-hole potential which can modify electronic energy levels compared to the single-particle DOS. In contrast, ARPES directly provides the energy- and momentum-resolved single-particle DOS with respect to E_F. The remarkable consistency with band dispersions observed in the present study as a function of doping confirms the validity of ARPES. We observed no additional

structure at a binding energy of 1.3 eV in the occupied DOS. In optimally doped high-temperature superconductors, the smaller bandwidth of the band crossing E_F compared to the band calculations has been reported and attributed to electron correlation effects[19]. This is in sharp contrast to heavily boron-doped diamond, where the experimental bandwidth is even slightly wider than that from calculations. This suggests a negligible role for the correlation effect in heavily boron-doped diamond.

The results revealed an overall occupied electronic structure directly related to the metallicity of the heavily boron-doped diamond superconductor. This provides experimental support for the very recent theoretical studies[7–9] that adopt the band structure approach to understanding the electronic properties of doped diamond and related materials. An understanding of the electronic structure of heavily boron-doped diamond may also be important for developing diamond-based devices[10] that make use of the unique properties of diamond.

METHODS

Homoepitaxially grown heavily boron-doped (111) diamond films (BDD1, BDD2 and BDD3) were made using a microwave plasma assisted chemical vapour deposition (CVD) method as described elsewhere[4,11]. T_c of 7.0 K of BDD1 was confirmed by the measurement of the onset of magnetization after the present photoemission measurements. The T_c determined from the onset of magnetization is lower than that measured for the onset of resistivity and normally corresponds to zero resistivity. BDD2 and BDD3 did not show onset of magnetization above 1.7 K. However, BDD2 showed onset of resistivity measured below 2.5 K. SIMS measurements for films (BDD1, BDD2, BDD3) made under the same conditions as the samples we used gave boron concentrations of 8.37×10^{21}, 1.18×10^{21} and 2.88×10^{20} cm^{-3}, respectively.

SXARPES measurements were performed at BL25SU, SPring-8, on a spectrometer built using a Scienta SES200 electron analyser. The energy and angular resolution were set to ~ 250 meV and $\pm 0.1°$ (corresponding to ± 0.026 Å^{-1}) for a photon energy of 825 eV, respectively, to obtain a reasonable count rate. Samples were cooled using a closed-cycle He refrigerator. Sample T was measured using a chromel-AuFe thermocouple mounted close to the sample. The base pressure of the spectrometer was better than 3×10^{-8} Pa. The sample orientation was measured ex situ using Laue photography. Location of the Γ point with respect to the measured ARPES data as well as the E_F position in the calculated spectra are determined by comparison between the experimental and calculated band dispersions near E_F. All measurements have been done for surfaces prepared with annealing at 400 °C to reduce oxygen contamination at the surface. E_F of the samples was referenced to that of a gold film evaporated onto the sample substrate measured just after the sample measurements. The measured k positions are determined with a free-electron final-state model by taking the photon momentum into consideration.

Band structure calculations for diamond are carried out within the local density approximation to the density functional theory. Kohn–Sham equations are solved self-consistently with the all-electron full-potential linear-augmented plane-wave (LAPW) method. The lattice constant of the face-centred cubic (f.c.c.) diamond structure is assumed to be 3.56 Å. The 'muffin-tin' sphere radius is taken as $R = 0.75$ Å. The LAPW basis functions up to $RK_{max} = 7.8$ are used to expand the wavefunctions.

1. Ashcroft, N. W. & Mermin, N. D. *Solid State Physics* Ch. 28, 561–587 (Saunders College, Fortworth, 1976).
2. Mott, N. *Metal-Insulator Transitions* Ch. 5, 145–169 (Taylor & Francis, London, 1990).
3. Bustarret, E., Gheeraert, F. & Watanabe, K. Dependence of the superconducting transition temperature on the doping level in single-crystalline diamond films. *Phys. Rev. Lett.* 93, 237005 (2004).
4. Ekimov, E. A. *et al.* Superconductivity in diamond. *Nature* 428, 542–545 (2004).
5. Takano, Y. *et al.* Superconductivity in diamond thin films well above liquid helium temperature. *Appl. Phys. Lett.* 85, 2851–2853 (2004).
6. Baskaran, G. Resonating valence bond mechanism of impurity band superconductivity in diamond. Preprint at 〈http://arXiv.org/cond-mat/0404286〉 (2004).
7. Boeri, L., Kortus, J. & Andersen, O. K. Three-dimensional MgB$_2$-type superconductivity in hole-doped diamond. *Phys. Rev. Lett.* 93, 237002 (2004).
8. Lee, K.-W. & Pickett, W. E. Superconductivity in boron-doped diamond. *Phys. Rev. Lett.* 93, 237003 (2004).